27-3-2024

Mathematical Analysis of the Electromotive Induced Force in a Magnetically Damped Suspension

Susana Aberturas

Juan Diego Aguilera

José Luis Olazagoitia
Universidad de Diseño, Innovación y Tecnología, UDIT

Miguel Ángel García

Antonio Hernando

Recommended Citation

Aberturas, S.; Aguilera, J.D.; Olazagoitia, J.L.; García, M.Á.; Hernando, A. Mathematical Analysis of the Electromotive Induced Force in a Magnetically Damped Suspension. Mathematics 2024, 12, 1004. https://doi.org/10.3390/ math12071004

mathematics

MDPI

Review

Mathematical Analysis of the Electromotive Induced Force in a Magnetically Damped Suspension

Susana Aberturas [1,*], Juan Diego Aguilera [2], José Luis Olazagoitia [3], Miguel Ángel García [4] and Antonio Hernando [2,5,6,7]

[1] Micromag 2000 SL, Avenida de Arroyomolinos, 3 y 5, P.L. Ventorro del Cano, 28925 Alcorcón, Spain
[2] Instituto de Magnetismo Aplicado (IMA), Universidad Complutense de Madrid-Administrador de Infraestructuras Ferroviarias (UCM-ADIF), 28230 Las Rozas, Spain; juandiag@ucm.es (J.D.A.); antherna@ucm.es (A.H.)
[3] Faculty of Design, Innovation and Technology, University of Design, Innovation and Technology (UDIT), Av. Alfonso XIII, 97, 28016 Madrid, Spain; joseluis.olazagoitia@udit.es
[4] Instituto de Cerámica y Vidrio, Campus de Cantoblanco, Consejo Superior de Investigaciones Científicas (CSIC), 28049 Madrid, Spain; magarcia@icv.csic.es
[5] Donostia International Physics Center, 20028 Donostia, Spain
[6] IMDEA Nanociencia, 28049 Madrid, Spain
[7] Engineering Department, Nebrija University, Sta. Cruz de Marcenado, 27, 28015 Madrid, Spain
* Correspondence: saberturas@micromag.es

Abstract: This study explores the advanced mathematical modeling of electromagnetic energy harvesting in vehicle suspension systems, addressing the pressing need for sustainable transportation and improved energy efficiency. We focus on the complex challenge posed by the non-linear behavior of magnetic flux in relation to displacement, a critical aspect often overlooked in conventional approaches. Utilizing Taylor expansion and Fourier analysis, we dissect the intricate relationship between oscillation and electromagnetic damping, crucial for optimizing energy recovery. Our rigorous mathematical methodology enables the precise calculation of the average power per cycle and unit mass, providing a robust metric for evaluating the effectiveness of energy harvesting. Further, the study extends to the practical application in a combined system of passive and electromagnetic suspension, demonstrating the real-world viability of our theoretical findings. This research not only offers a comprehensive solution for enhancing vehicle efficiency through advanced suspension systems but also sets a precedent for the integration of complex mathematical techniques in solving real-world engineering challenges, contributing significantly to the future of energy-efficient automotive technologies. The cases reviewed in this article and listed as references are those commonly found in the literature.

Keywords: electromagnetic damping; Energy Harvesting Shock Absorbers (EHSAs); induced electromotive force; non-lineal magnetic flux; power; mathematical description

MSC: 78M16

Citation: Aberturas, S.; Aguilera, J.D.; Olazagoitia, J.L.; García, M.Á.; Hernando, A. Mathematical Analysis of the Electromotive Induced Force in a Magnetically Damped Suspension. *Mathematics* **2024**, *12*, 1004. https://doi.org/10.3390/math12071004

Academic Editor: Jacques Lobry

Received: 15 February 2024
Revised: 13 March 2024
Accepted: 20 March 2024
Published: 27 March 2024

1. Introduction

The increasing global energy demand and the corresponding rise in environmental concerns have catalyzed a shift towards sustainable and efficient energy usage, particularly in the automotive industry [1].

With the ongoing evolution towards electric vehicles, overcoming limitations such as low autonomy compared to fossil fuel vehicles has become a critical challenge [2].

A promising approach to address these limitations is through energy recovery systems, which not only enhance vehicle range but also reduce energy consumption and emissions [3]. The automotive industry faces increasing pressure to enhance energy

efficiency and reduce environmental impacts. The global shift towards electric vehicles emphasizes the necessity for innovative solutions to improve vehicle range and efficiency while addressing environmental concerns. Among various strategies, energy recovery systems have emerged as key technologies to enhance vehicle efficiency and sustainability, particularly in the context of vehicle suspension.

Regenerative braking systems [4], thermoelectric generators [5], and energy recovery from engine gases [6] represent significant advancements in this domain. However, these methods each have limitations and areas for improvement, particularly in the context of maximizing efficiency and applicability. Recently, attention has turned to the vehicle's suspension system as a novel source for energy recovery [7]. Traditional shock absorbers dissipate mechanical energy as heat, presenting an opportunity for energy recovery [8]. The concept of Energy-Harvesting Shock Absorbers (EHSAs) has been introduced as a means to convert lost kinetic energy from road irregularities into usable electrical energy, potentially increasing the overall efficiency of vehicles [9].

Various technologies have been proposed for EHSAs, including hydraulic EHSAs [10] which employ a pump and motor to convert mechanical to electrical energy and are capable of handling high forces, but are often bulky and complex. Piezoelectric materials [11] are more suitable for high-frequency applications but face challenges at lower frequencies typical of suspension systems.

Electromagnetic EHSAs have emerged as a promising technological solution, particularly for their compact design and potential for high energy recovery efficiency. These systems harness electromagnetic induction to generate electricity, but optimizing their energy conversion process remains a significant challenge [12]. These systems can be divided into linear and rotational electromagnetic generators [13], and systems that convert translational suspension movement into rotational motion, such as pinion–rack [14] or ball screw [15], among others.

Innovations in linear systems include the application of magnetic solutions using both hard and soft magnetic materials in dampers, and these have been explored to overcome existing limitations and enhance the efficiency of electromagnetic EHSAs [16]. These systems utilize the interaction between magnets and coils to convert motion into electrical energy. The design and efficiency of these systems depend heavily on the positioning and characteristics of the magnets and coils [17], making it challenging to assess and optimize these technologies [18]. Despite this, the potential of electromagnetic systems in converting suspension activity into electrical energy is considerable. Not only do they offer a means of energy recovery, but they also enable the transformation of passive suspension systems into active ones, allowing for adjustable operating characteristics [19].

An important aspect of designing effective electromagnetic suspension systems is understanding the relationship between the magnet's position and the amount of energy that can be collected using the coil [20]. This relationship is crucial for optimizing the system's efficiency, as the energy collected depends on the coil's position relative to the magnet.

One critical gap in current research is the lack of a comprehensive understanding of the dynamics governing magnetic suspension systems and their potential for energy recovery. Traditional linear models fail to capture the complex behaviors of electromagnetic interactions in suspension systems, leading to inefficiencies and missed opportunities for energy recovery. Additionally, there is an absence of a standardized protocol for comparing different energy recovery systems, which hampers the assessment and optimization of these technologies [21].

This study aims to address these gaps by delving into the advanced mathematical and physical analysis of electromagnetic energy recovery within vehicle suspension systems. Specifically, it seeks to explore the dynamics of these systems beyond conventional linear models, employing techniques such as Taylor expansion and Fourier analysis to offer a more detailed and accurate understanding.

Furthermore, this research intends to bridge the theoretical and practical aspects of energy recovery, by not only examining the fundamental principles governing electromagnetic suspension systems but also by considering their real-world application and optimization. By analyzing combined passive and electromagnetic suspension systems and converting differential motion equations into algebraic ones, this study aims to provide valuable insights into the design and efficiency of energy recovery solutions.

In response to these challenges, the mathematics and physics underlying the electromagnetic energy harvesting obtained during car motion is reviewed in this article. In essence, this article intends to explore the sophisticated mathematical landscape of electromagnetic energy harvesting in vehicle suspension systems. It aims to shed light on the complex interactions and dynamics within these systems, offering a pathway to more efficient and effective energy recovery solutions. Through this rigorous analytical approach, the study contributes significantly to the broader goal of enhancing vehicle energy efficiency and sustainability in the automotive industry.

In Sections 2 and 3, the correlation between the oscillation and the electromagnetic damping is analyzed. As in many cases, the magnetic flux is not a linear function of the displacement, and the general procedure to solve the motion equation based on Taylor expansion and Fourier analysis is revisited. In the third section, the average power per cycle and unit mass is calculated and described. Finally, in Section 4, the study of a more technical and applied system is addressed, as is the combination of a passive and an electromagnetic suspension system, by using the Fourier analysis to convert the differential motion equations in algebraic equations.

2. Methodology

2.1. Equation of Motion and Electromagnetic Damping

Consider a magnet, hanging fixed at a spring that supports a mass, m, subject to an external force per unit mass $F(t)$, Figure 1. The magnet periodic motion, along the x axis, generates an induced electromotive force, E, in a stationary coil located at its proximity. By the relativity principle, the same physics governs the case in which the coil is fixed to the spring and the magnet remains stationary.

Let us call φ_0 the flux through the coil at the equilibrium position of the magnet $x_0 = a$. The induced electromotive force is then given by

$$E = -\frac{d\Phi}{dt} \tag{1}$$

Here, we neglect a contribution to the magnetic flux from magnetic materials or ambient fields, as they would require individual solutions. Exact solutions should be obtained considering these contributions, but the procedure is that presented here.

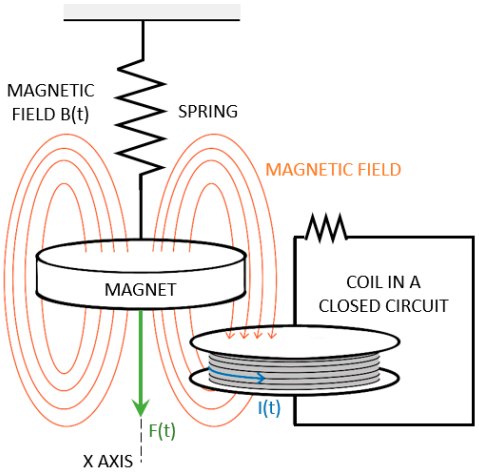

Figure 1. System composed of a magnet attached to a spring and in proximity to a collector coil.

Part of the power absorbed by the spring from the external force is used to support a current $I(t)$ in the circuit formed by the coil and the load resistance and is given by

$$P = \frac{d\left(E_{kin} + E_{pot}\right)}{dt} = f^*(t)x'(t) = \beta' x'(t)^2 \tag{2}$$

where $f^*(t)$ is the electromagnetic friction force opposite to the motion and β' its corresponding coefficient ($f^*(t) = \beta' x'(t)$). $f(t)$ can be written as the gradient of the work, $I(t)\Phi(t)$ given by the current

$$f^*(t) = -\frac{d\Phi}{dx} I(t) \tag{3}$$

If L and R are the induction coefficient and the resistance of the coil and R^* the resistance of the load, $I(t)$ is related to E through the following relationship

$$E = -\frac{d\Phi}{dt} = L\frac{dI(t)}{dt} + (R + R^*)I(t) \tag{4}$$

Then, (4) yields for $I(t)$

$$I(t) = -\frac{1}{(R + R^* + i\omega L)}\frac{d\Phi}{dt} = -\frac{1}{(R + R^* + i\omega L)}\frac{d\Phi}{dx}\frac{dx}{dt} \tag{5}$$

Then, according to (3) and (5), $f(t)$ becomes

$$f^*(t) = \beta' x'(t) = \frac{1}{(R + R^* + i\omega L)}\left(\frac{d\Phi}{dx}\right)^2 \frac{dx}{dt} \tag{6}$$

Thus, the magnet and thereby the spring should undergo, per unit mass, the reactive force associated with the induced electromotive force, given by $f(t) = \frac{f^*(t)}{m} = \frac{\beta'}{m} x'(t) = \gamma' x'(t)$.

The real and imaginary components of γ', according to (6), are given by

$$\begin{aligned} \gamma'_r &= \frac{(R + R^*)}{m((R + R^*)^2 + (\omega L)^2)}\left(\frac{d\Phi}{dx}\right)^2 \\ \gamma'_i &= \frac{-\omega L\left(\frac{d\Phi}{dx}\right)^2}{m((R + R^*)^2 + (\omega L)^2)} \end{aligned} \tag{7}$$

The equation of the spring motion can then be written as a function of the external force $F(t)$ per unit mass as

$$x'' + (\gamma + \gamma')x' + \omega_0^2 \mathrm{x} = \int_{-\infty}^{\infty} F(\omega) cos\omega t \, \mathrm{d}\omega \tag{8}$$

where the term γ is the mechanical friction coefficient of the spring motion and $F(\omega)$ the Fourier transform of the applied force per unit mass $F(t)$.

The Fourier expansion of $x(t)$ yields

$$x(\omega) = \frac{F(\omega)}{\omega_0^2 - \omega^2(1 - \frac{\gamma'_i}{\omega}) + i\omega(\gamma + \gamma_r)} \tag{9}$$

Equation (9) illustrates the action of both self-inductance and resistance on the motion equation; the first one introduces a mass correction whereas the total resistance of the secondary circuit, coil plus load, acts as an additional friction term.

The dissipative coefficient consists of two terms, one due to the mechanical friction γ and the other due to a new one γ'_r or electromagnetc friction coefficient.

In many cases, the oscillation frequency is sufficiently low (a few cycles per second) to disregard the term proportional to L. Subsequently, Equation (8) simplifies since $\gamma'_i = 0$ and $\gamma'_r = \frac{1}{m(R+R^*)}\left(\frac{d\Phi}{dx}\right)^2$, therefore $x(\omega)$ can be expressed as

$$x(\omega) = \frac{F(\omega)}{\omega_0^2 - \omega^2 + i\omega\left(\gamma + \frac{1}{m(R+R^*)}\left(\frac{d\Phi}{dx}\right)^2\right)} \tag{10}$$

Notice that if the flux Φ is proportional to x, i.e., $\left(\frac{d\Phi}{dx}\right) = a$, the term γ' is a constant and can be added to the mechanical friction coefficient γ to yield a total friction coefficient $\gamma^* = \gamma + \gamma' = \gamma + \frac{a^2}{m(R+R^*)^2}$

When the derivative $\left(\frac{d\Phi}{dx}\right)$ can not be properly approximated to a linear function of x, γ' ceases being a constant and Equation (7) loses its linear character.

Finally, it is worth to note that the electromagnetic power available to be used by the load, $I^2 \times R^*$, according to (5) and for a constant electromotive force induced in the pick-up coil, reaches a maximum for $R = R^*$. If the induction coefficient L is not disregarded the maximum corresponds with more generality to $Z = Z^*$, or the matching condition between the load, Z^*, and the pick-up coil, Z, impedances.

2.2. Taylor Expansion of $\left(\frac{d\Phi}{dx}\right)$ *and Fourier Analysis*

2.2.1. Taylor Expansion

Before analyzing some simple cases let us outline a general treatment of the problem by using the Taylor expansion of the flux around the equilibrium position of the magnet, $x = x_0$. This procedure leads to the following relationship

$$\Phi(x) = \Phi(x_0) + \sum_{n=1}^{\infty} \frac{1}{n!}\left(\frac{d^n\Phi}{dx^n}\right)_{x=x_0} (x - x_0)^n \tag{11}$$

Therefore, the term $\left(\frac{d\Phi}{dx}\right)^2$ that appears in Equations (6) and (7) in the expressions of γ◎becomes (taking $x_0 = 0$):

$$\left(\frac{d\Phi}{dx}\right)^2 = \left(\sum_{n=1}^{\infty}\sum_{p=1}^{\infty} \frac{1}{(p-1)!}\frac{1}{(n-1)!}\Phi_n\Phi_p x^{n+p-2}(t)\right) \tag{12}$$

Consequently, $\left(\frac{d\Phi}{dx}\right)^2 \frac{dx}{dt}$ may be written as

$$\left(\frac{d\Phi}{dx}\right)^2 \frac{dx}{dt} = \left(\sum_{n=1}^{\infty}\sum_{p=1}^{\infty} \frac{1}{(p-1)!}\frac{1}{(n-1)!}\frac{1}{(n+p-1)}\Phi_n\Phi_p \frac{d}{dt} x^{n+p-1}(t)\right) \tag{13}$$

In summary, in the general case, γ' is not a constant but an expansion of increasing powers of the position x [22]. Note that when the magnet oscillates between two points for which the distance to the coil is maximum and minimum, respectively, the flux could be roughly approximated using a linear function of x. In this case, γ' is a constant and the motion equation has a solution that is the well-known solution of the harmonic oscillator. However, when the rest position corresponds to the maximum flux, i.e., $\Phi(0)$ in (11) is maximum, the γ' coefficient is at least proportional to x^2, as shown in one of the examples studied below.

The approximation degree of the expansion must be tuned by considering the particular expected shape of the function $\Phi(x)$, the distance between the pick-up coil and the primary field source, as well as the amplitude of the oscillation.

2.2.2. Fourier Analysis

As we have to deal with the powers of $x(t)$, as indicated by (11) and taking into consideration that the real part of any power of $e^{i\omega t}$ is different to the same power of $x(t)$, it is more suitable to express $x(t)$ as

$$x(t) = \frac{1}{2\pi}\int_0^{\infty} x(\omega)\cos\left(\omega t + \varphi(\omega)\right)d\,\omega \tag{14}$$

According to (7), the equation of motion (6) can be written in the frequency domain once that the Fourier transform of $\gamma' x'$ has been determined.

Taking into account the Fourier transform of $\frac{d}{dt}cos^n\left(\omega t + \varphi(\omega)\right)$, the $\left(\frac{d\Phi}{dx}\right)^2\frac{dx}{dt}$ can be expanded

$$\begin{aligned}\left(\frac{d\Phi}{dx}\right)^2\frac{dx}{dt} = & -\omega(A(1)\sin(\omega t + \varphi(\omega)) + A(2)\sin 2(\omega t + \varphi(\omega) + \\ & A(3)\sin 3(\omega t + \varphi(\omega)) + \cdots =\end{aligned} \tag{15}$$

$$\begin{aligned} A(1) &= -\omega\left(\phi_1^2 x(\omega) + \frac{1}{3}(\phi_1\phi_3 + \phi_2^2)x^3(\omega) + \cdots\right) \\ A(2) &= -\omega\left(\phi_1\phi_2 x^2(\omega) + \frac{1}{4}(\phi_2\phi_3 + \frac{1}{3}\phi_1\phi_4)x^4(\omega) + \cdots\right) \\ A(3) &= -\omega\left(\frac{1}{4}(\phi_1\phi_3 + \phi_2^2)x^3(\omega) + \cdots..\right)\end{aligned} \tag{16}$$

In conclusion, the equation of motion in the frequency domain generally becomes nonlinear and, thereby, it has not any closed form solution. Therefore, numerical procedures such as the Runge–Kutta method should be applied to the different particular motion conditions.

2.2.3. Example: A Particular Geometry for the Coil-Magnet System for Which $\Phi(0)$ Is Maximum or $\left(\frac{d\Phi}{dx}\right)_{x=0} = 0$

In Figure 2b, the poles of the magnet are in front of a circular coil surface in such a way that the flux through the coil surface is maximum, i.e., $\Phi(0)$ in (10) is maximum [23]. Appendix A presents the calculations for the case of rectangular poles structure. After assuming that the magnetic field lines, B, are restricted to the magnet surface, the flux through the n-turns coil becomes $nBS(x)$, where $S(x)$ is the intersection of both the magnet and the coil surfaces and depends on the cantilever displacement, x.

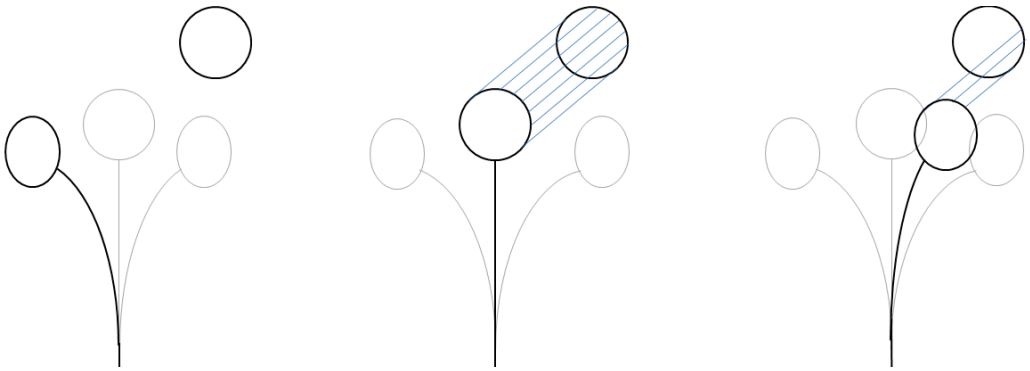

(**a**) (**b**) (**c**)

Figure 2. Cylindrical magnet glued to the free end of a cantilever that oscillates around its equilibrium position. (**a**) there is no intersection of the flux between magnet and coil; (**b**) shows how the intersection is equal to the entire surface of *S(x)*; (**c**) shows how there is only intersection in a fraction of the surface of $S(x)$.

The induced electromotive force (2) is then given by

$$E = -\frac{d\Phi}{dt} = -nB\frac{dS(x)}{dx}\frac{dx}{dt} = -nB\sqrt{4r^2 - x^2}\frac{dx}{dt} \tag{17}$$

where r is the coil radius assumed to be equal to that of the magnet surface. Accordingly, the motion Equation (8) becomes

$$x'' + \left(\gamma + \frac{n^2B^2}{m(R+R^*)}(4r^2 - x^2)\right)x' + \omega_0^2 x = \int_{-\infty}^{\infty} F(\omega)cos\omega t \, d\omega \quad (18)$$

where we have disregarded the self-inductance term of the circuit.

This may also be expressed as

$$x'' + \gamma^* x' - \frac{n^2B^2}{m(R+R^*)}x^2x' + \omega_0^2 x = \int_{-\infty}^{\infty} F(\omega)cos\omega t \, d\omega \quad (19)$$

where γ^* holds for the constant $\gamma^* = \gamma + \frac{n^2B^2}{m(R+R^*)}4r^2$.

According to the assumed B lines distribution around the magnet, the magnet motion induces electromotive force as its displacement and x is restricted to be smaller than $2r$ [24].

For $x \leq 2r$, the equation of motion can then be approximated by

$$x'' + \gamma^* x' - \omega_0^2 x = \int_{-\infty}^{\infty} F(\omega)cos\omega t \, d\omega \quad (20)$$

with $\gamma^* = \gamma + \alpha\frac{n^2B^2}{m(R+R^*)}r^2$ where α is a fitting parameter comprised between 3 and 4.

For $x \geq 2r$, the following motion equation holds that

$$x'' + \gamma x' - \omega_0^2 x = \int_{-\infty}^{\infty} F(\omega)cos\omega t \, d\omega \quad (21)$$

In order to estimate the error associated with the use of the simplified Equation (20), its corresponding analytical solution has been compared with that numerically obtained for the nonlinear Equation (19) by using the Runge–Kutta method, as shown in Figure 3. The excellent match between the solution of the original equation and the used approximation confirms the reliability of this later.

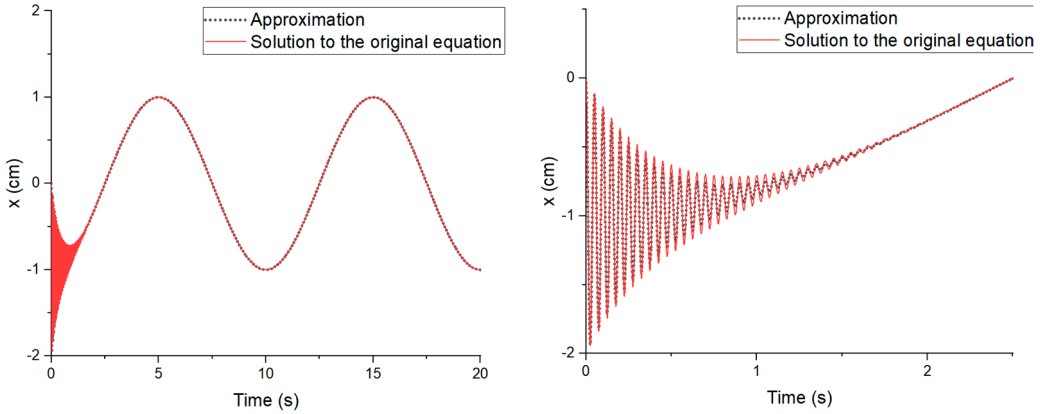

Figure 3. Comparison in amplitude of the solution to the original equation and the approximated solution for ω = 0.1 Hz. (**a**) Figure between 0 and 20 s; (**b**) by zooming in on (**a**), the area of the graph between 0 and 2 s can be seen more clearly (see Appendix B for details).

3. Electromagnetic Energy Harvested during Spring Motion

The instantaneous electromagnetic power harvested through unit mass is given by $\gamma' x'^2$, and taking into account Equations (7) and (9), we find for the average power in a cycle

$$\langle P(\omega)\rangle = \frac{\frac{1}{2}\gamma'_r F_\omega^2 \omega^2}{\left((\omega_0^2 - \omega^2(1 - \frac{\gamma'_i}{\omega})\right)^2 + \omega^2(\gamma + \gamma'_r)^2} \quad (22)$$

In order to estimate the relative values of the real and imaginary components of γ, let us consider a circular pick-up coil with the radius r and height l made with a wire of resistivity ρ and cross section S. It is easy to find that

$$\frac{\gamma'_i}{\gamma'_r} = \omega\frac{L}{R} = \omega\frac{\mu_0\mu_r n^2\pi r^2}{l\frac{2\pi r n\rho}{S}} = \omega\frac{\mu_0\mu_r nrS}{2\rho l} \approx \omega\frac{\mu_0\mu_r S}{4\rho} \quad (23)$$

where the last term was obtained by assuming that $l \approx 2rn$.

According to (23), when $\mu_r = 200, s = 3\text{ x }10^{-8}\text{ m}^2$ and $\rho = 5\text{ x }10^{-8}\,\Omega$m, the ratio $\frac{\gamma'_i}{\gamma'_r}$ approximately becomes $3.6\text{ x }10^{-5}\omega$. Therefore, when the frequency is kept below 1 kHz, γ'_i can be disregarded, and Equation (22) may be rewritten in a simplified form as

$$\langle P(\omega)\rangle = \frac{\frac{1}{2}\gamma'_r F_\omega^2 \omega^2}{((\omega_0^2 - \omega^2)^2 + \omega^2(\gamma + \gamma'_r)^2} \quad (24)$$

Since in EHSA frequencies higher than 100 Hz are generally absorbed through other elements such as tires, $\omega < 1$ kHz does not restrict us and it is always acceptable to disregard γ'_i term.

Moreover, when $\left(\frac{d\Phi}{dx}\right) = a$, $\langle P(\omega)\rangle$ may be expressed as:

$$\langle P(\omega)\rangle = \frac{\frac{a^2}{2m(R+R^*)}F_\omega^2\omega^2}{((\omega_0^2 - \omega^2)^2 + \omega^2\left(\gamma + \frac{a^2}{m(R+R^*)}\right)^2} \quad (25)$$

The forces involved in the process of energy harvesting during car motion have Fourier components of a few Hz, therefore Expression (25) is generally correct. Furthermore, the applied force is due to the road roughness x_l, which contracts the spring and consequently can be written per unit mass as $F_\omega = -\omega_0^2 x_l(\omega)$. Notice that the Fourier components of x_l are functions of the wavelength, λ, of the road roughness, therefore, for a given λ, the corresponding ω depends on the speed of the car, v, as $\omega = \frac{2\pi}{\lambda}v$. On the other hand, the constant a^2, by its definition, can be approximated to $\frac{(nSB)^2}{(2r)^2} \approx \frac{(n\pi rB)^2}{4}$, where n and S are the number of turns and the cross section of the pick-up coil, respectively, B is the average value of the magnetic field taken over all the points of the coil cross section at the rest position ($x = 0$) of the magnet and r the radius of the coil. It has been assumed that the flux evolves from its maximum value nSB at $x = 0$ to zero at $x(t) = 2r$, r being the coil radius. After taking all these points into consideration, Equation (25) becomes

$$\begin{aligned}\langle P(\omega)\rangle &= \frac{\frac{(nSB)^2\omega_0^4\omega^2}{8m(R+R^*)r^2}x_{l\omega}^2}{((\omega_0^2 - \omega^2)^2 + \omega^2\left(\gamma + \frac{(nSB)^2}{4mr^2(R+R^*)}\right)^2} \\ &= \frac{\frac{(n\pi rB)^2\omega_0^4\omega^2}{8m(R+R^*)}x_{l\omega}^2}{((\omega_0^2 - \omega^2)^2 + \omega^2\left(\gamma + \frac{(n\pi rB)^2}{4m(R+R^*)}\right)^2}\end{aligned} \quad (26)$$

Consider a system in which the radius of the coil is $r = 0.5$ cm or S ≈ 8×10^{-5} m^2, and the number of turns $n = 1000$, $B = 1$ T. The mass is $m = 2$ kg and the mechanical friction $\gamma = 4$ Ns/kg·m, the total resistance of the secondary circuit is $R + R^* = 20\ \Omega$, and ω_ϑ =20 Hz.

According to these values, the electromagnetic damping verifies $\gamma'_r = \frac{(n\pi rB)^2}{4m(R+R^*)} = 0.035$ Ns/kg·m. The average power as a function of ω is then, according to (26), that shown in Figure 4a. If the number of turns as well as the coil radius increases up to a factor two, γ'_r increases up to 0.56 (disregarding the increase in electric resistance) and the corresponding dependence of the power with frequency is illustrated by Figure 4b. Both curves were obtained from (26) after assuming $x_{l,\omega} = 2r$.

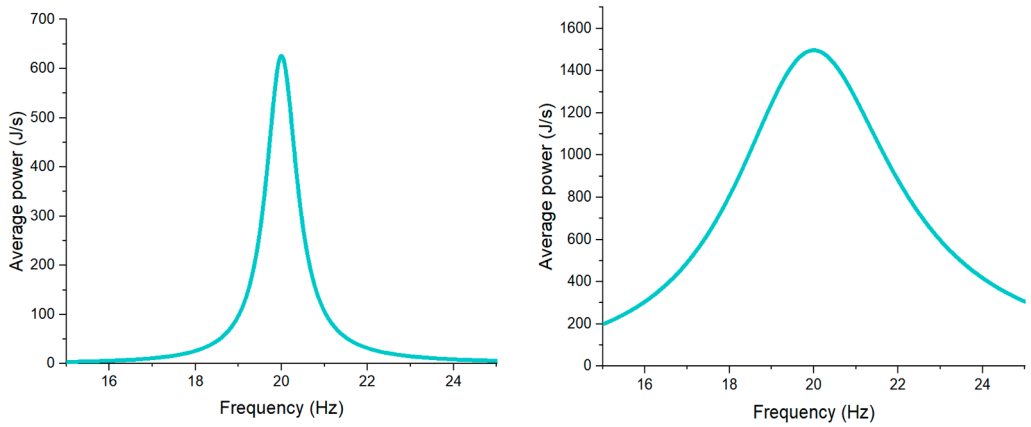

(**a**) (**b**)

Figure 4. (**a**) Average power as a function of ω; (**b**) average power as a function of ω increasing the number of turns as well as the coil radius up to a factor two.

As an example, let us consider a x_l profile that as a function of time is a rectangular pulse of width $2t_0 = 2d/v$, where v is the car speed. It can then be written:

$$x_l(t) = \int_{-\infty}^{\infty} x_l(\omega) e^{i\omega t}\, \mathrm{d}\omega \tag{27}$$

where

$$x_l(\omega) = \frac{2x sin\omega t_0}{\omega} \tag{28}$$

Therefore, $x_l(\omega)$ becomes negligible for frequencies below $\omega_l = \frac{3\pi}{2t_0} = \frac{3\pi v}{4d}$. The limit value $\omega_l = \frac{3\pi v}{4d}$ correponds to the maximum frequency for which the Fourier transform of the applied force takes significant values. If the resonance frequency shown in Figure 4 is higher than ω_l, the power absorption would be very low. But an increase in the car speed v would approach ω_l to the resonance and the system will start to harvest considerable power. For instance, if d = 0.2 m, as the resonance frequency is ω_0 = 20 Hz, the speed required to reach ω_l = 20 Hz is 6 km/h.

It is important to remark that the increase in power absorbed through the electromagnetic system is achieved when increasing the oscillation amplitude of the system finds a counterpart in the corresponding decrease in comfort. Jiang et al. [24] have studied with detail some of these correlations.

Finally, it must be indicated that, according to (24), the maximum power absorbed using the electric circuit, when the strength and frequency of the force remain constant, corresponds to an electromagnetic friction coefficient given by $\gamma'^2_r = \gamma^2 - \frac{(\omega_0^2-\omega^2)^2}{\omega^2}$. Note that the maximum electromagnetic power absorption at the mechanical resonance requires that $\gamma'_r = \gamma$, i.e., the matching of mechanical and electrical impedances.

4. Motion Equations and Electromagnetic Power Absorbed in an Energy Harvesting Suspension Formed Using a Combination of a Passive Suspension Plus an Electromagnetic One

As indicated by Jiang et al. [24], an energy harvesting suspension can be formed using a passive suspension that consists of a spring and a damper, and via an energy harvester consisting of a system of magnets and coils. The magnets can be fixed to the cylinder linked to the wheel axis, or lower cover, whereas the coils are fixed to the upper mass of the car or upper cover and can move in the magnetic field.

The equation of motion can be written as

$$\begin{gathered} m_1 x''_1 + k_1(x_1 - x_2) + c(x_1' - x_2') - k_a i = 0 \\ m_2 x''_2 + k_2(x_2 - x_l) - k_1(x_1 - x_2) - c(x_1' - x_2') + k_a i = 0 \\ Li' + Ri + k_a(x_1' - x_2') = 0 \end{gathered} \tag{29}$$

The magnetic flux through the coil is assumed to be proportional to the displacement between the magnet and the coil as is the case studied in previous Section 3.

m_1 is the car or sprung mass, m_2 is the wheel and wheel axes mass or unsprung mass, k_1 and c are the stiffness and damping coefficient of the passive suspension, k_2 is the tire stiffness, k_a is the electromagnetic coupling coefficient, and x_1, x_2 and x_l are the displacements of the sprung vehicle mass, the unsprung mass and the road profile, respectively.

The system of differential Equation (29) is turned into a set of algebraic equations through the Fourier transform. The driving force is due to the road profile that can be written as $x_l = \int_{-\infty}^{\infty} x_l(\omega) e^{i\omega t}\, d\omega$. Then, for a particular $x_l(\omega)$, Equation (29) becomes

$$\begin{gathered} (-m_1\omega^2 + k_1 + i\omega(c + \frac{k_a}{R + i\omega L}))x_1(\omega) + (-k_1 - i\omega(c + \frac{k_a}{R + i\omega L}))x_2(\omega) = 0 \\ (-k_1 - i\omega\left(c + \frac{k_a}{R + i\omega L}\right)x_1(\omega) + (-m_2\omega^2 + k_1 + k_2 + i\omega(c + \frac{k_a}{R + i\omega L}))x_2(\omega) = k_2 x_l(\omega) \end{gathered} \tag{30}$$

After defining

$\alpha_1 = -m_1\omega^2;\ \alpha_2 = -m_2\omega^2 + k_2;\ \beta = k_1 + i\omega(c + \frac{k_a}{R + i\omega L})$

Equation (30) can be rewritten as

$$\begin{gathered} (\alpha_1 + \beta)x_1(\omega) - \beta x_2(\omega) = 0 \\ -\beta x_1(\omega) + (\alpha_2 + \beta)x_2(\omega) = k_2 x_l(\omega) \end{gathered} \tag{31}$$

The solutions are

$$\begin{gathered} x_1(\omega) = \frac{k_2\beta}{(\alpha_1 + \beta)(\alpha_2 + \beta) - \beta^2} x_l(\omega) \\ x_2(\omega) = \frac{k_2(\alpha_1 + \beta)}{(\alpha_1 + \beta)(\alpha_2 + \beta) - \beta^2} x_l(\omega) \end{gathered} \tag{32}$$

Equation (30) leads to the following relationship

$$x'_1 - x'_2 = i\omega \frac{m_1\omega^2 k_2}{m_1 m_2\omega^4 - m_1 k_2\omega^2 + (k_2 - m_1\omega^2 - m_2\omega^2)\left(k_1 + i\omega\left(c + \frac{k_a}{R + i\omega L}\right)\right)} x_l \tag{33}$$

By assuming the term ωL to be negligible respect to R, it can be written as

$$x'_1 - x'_2 = \frac{R m_1\omega^3 k_2}{\left(\omega(k_2 - m_1\omega^2 - m_2\omega^2)(cR + k_a)\right) - iR(m_1 m_2\omega^4 - m_1 k_2\omega^2 + (k_2 - m_1\omega^2 - m_2\omega^2)k_1)} x_l \tag{34}$$

The amplitude of the electromagnetic power harvested during a cycle by the motion of the system is, according to Equation (22), given by

$$P = \frac{K_a^2}{R}|x'_1 - x'_2|^2 \tag{35}$$

That according to (34) yields

$$P = \frac{k_a^2 R(m_1\omega^3 k_2)^2}{\left(\omega(k_2 - m_1\omega^2 - m_2\omega^2)(cR + k_a)\right)^2 + (R(m_1 m_2\omega^4 - m_1 k_2\omega^2 + (k_2 - m_1\omega^2 - m_2\omega^2)k_1)^2} x_l^2 \tag{36}$$

Figure 5 depicts the power absorbed as a function of frequency, when the calculation was performed for the following parameters: $m_1 = 2$ kg; $m_2 = 4.2$ kg; $k_1 = 5 \times 10^3$ N/m; $k_2 = 3 \times 10^3$ N/m; $R = 20\ \Omega$; C = 16 N.s/m; $k_a = 34$ T.m., those values have been considered before by Jiang et al. [24]. It was also considered $x_l = 1$ mm.

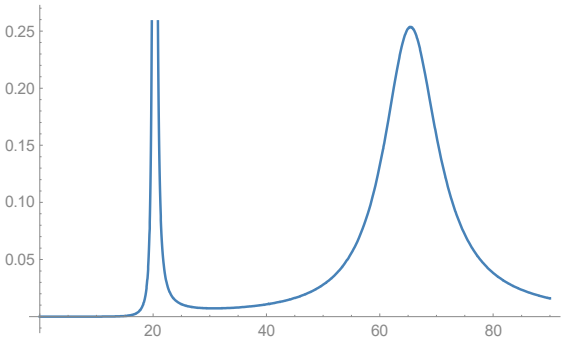

Figure 5. Average power as a function of ω with specific parameters.

The observed maximum corresponds to the resonant frequencies that are those for which one of the terms of the denominator in Equation (31) vanishes., i.e., $\omega_1 = \sqrt{\frac{k_2}{m_1+m_2}} \approx 21$ Hz and $\omega_2 = \sqrt{\frac{k_1+k_2}{2m_2} + \frac{k_1}{2m_1} \pm \sqrt{\left(\frac{k_1+k_2}{2m_2} + \frac{k_1}{2m_1}\right)^2 - \frac{k_1 k_2}{m_1 m_2}}} \approx 69$ Hz.

5. Soft Magnetic Nucleus within the Pick-Up Coil

A possible way to increase the harvested electromagnetic power is to wind the pick-up coil around a soft magnetic nucleus that could act as flux multiplier [25]. In the expressions written above, in which appears the average magnetic field strength over the surface closed by the coil, B, it is assumed that the coil has been wound around air. In this case, B can be expressed as $B = \mu_0 H$, where H is the magnetic field strength in Am^{-1} and μ_0 the vacuum magnetic permeability that takes the value $4\pi 10^{-7}$ Hm^{-1}. However, when the coil is wound around a soft magnetic nucleus, the expression of B changes to the following one:

$$B = \mu_0(H + M) = \mu_0(H_a + H_d + M) \tag{37}$$

H being now the sum of both applied H_a and demagnetizing H_d fields. By using the demagnetizing factor approximation, the following relationship for the demagnetizing field is obtained: $H_d = -NM$.

The magnetization of the nucleus is formally related to the applied field according to $M = \chi H$ that, after taking into account the two above mentioned H components, leads to the relation

$$M = \frac{\chi}{1 + \chi N} H_a \tag{38}$$

This last expression indicates that the magnetization of the soft material induced by the action of the field created via the magnet decreases as the demagnetizing factor of the

soft nucleus increases. This decrease is more remarkable as the soft material susceptibility is higher.

Figure 6 shows the scheme of the magnet and the coil. In order to estimate the orders of magnitude of the involved physical properties, let us consider a cylindrical magnet with radius r and a cylindrical coil with the same radius. The nucleus is a cylinder also with a radius r and thickness h, as illustrated in Figure 6. The thickness must be conditioned by the thickness of the coil, otherwise a large volume must be required to accommodate the system.

In the model of soft material core, hysteresis has been neglected in order to provide an analytical solution, making such a model just to be approximated (i.e., the core is considered to be an ideal soft ferromagnet).

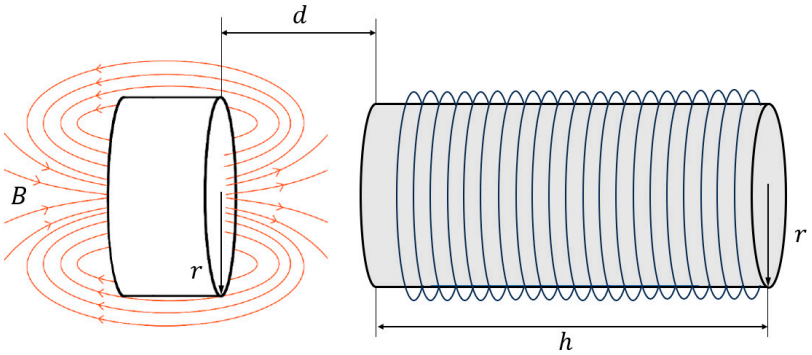

Figure 6. Magnet at a distance d from the coil with also cylindrical-shaped nucleus.

The demagnetizing factor of a cylinder along its axis depends on the aspect ratio, k, which is the ratio of length to diameter, $k = h/2r$. For $k = 1$, N is 0.27 and for $k = 2$, $N = 0.14$ [26]. If we call d the minimum distance between the magnet surface and the nucleus surface (see Figure 6), the magnetic field strength produced by the magnet, H_a, must be averaged between d and $d + h$. As d increases, H_a also does as its average decreases, but the demagnetizing field in the nucleus also decreases when $H_a < NM_s$. According to these qualitative changes depicted by Expression (38), the nucleus magnetization shows a competitive influence of both effects.

Notice that the maximum efficiency of the nucleus is achieved when $H_a > NM_s$ (assuming that the coercive field of the soft material is negligible), NM_s being the maximum demagnetizing field, where M_s holds for the nucleus saturation magnetization. Under this condition, the average B across the coil is roughly given by $B = (N + 1)M_s$. The maximum B is then comprised between M_s and $2M_s$. Let us consider $r = 1$ cm and $k = 2$ and the saturation magnetization of the soft nucleus 1 T. The maximum demagnetizing field is then 0.14 T. The field produced by the magnet must be $\mu_0 H_a > 0.14$ T. As $k = 2$, the distance of the basis of the soft magnetic cylinder to the magnet surface cannot be smaller than 4 cm (case of $d = 0$). For this distance, the field produced by the magnet is lower than 0.1 T for any magnet with a saturation magnetization of the order of 1.5 T.

If the aspect ratio k is 1 then $h = 2$ cm and the maximum demagnetizing field becomes 0.28 T. But the field produced by the magnet at 2 cm is of the order of 1.5 T. It can be concluded that for the scheme depicted by Figure 6, which is the more often used in an energy harvesting system, filling the coil with a soft ferromagnetic nucleus can only weakly increase the magnetic flux and thereby the harvested power. In any case, the overall increase cannot be higher than the corresponding to a factor two.

It is obvious that when the system is not restricted to the conditions fixed by the scheme illustrated in Figure 6, the effect of the magnetic nucleus may be noticeable, as has been studied for a different configuration [22,25].

6. Conclusions

In conclusion, this investigation into the non-linear dynamics of magnetic flux in relation to displacement has not only highlighted a significant gap in current research but has also provided a robust mathematical framework to address this challenge. The employment of Taylor expansion and Fourier analysis has proven to be a pivotal approach in understanding and optimizing the correlation between oscillation and electromagnetic damping. This has enabled us to develop a comprehensive model that accurately calculates the average power per cycle and unit mass, a crucial step in quantifying the efficiency of energy harvesting in suspension systems.

Relationships as those described by (24), (26) or (36) enable the ideal design of the electrical circuit according to the oscillator conditions. The use of these expressions leads to deep information about the possible energy fractions that can be harvested and offers the ability to control this percentage through tuning the corresponding impedance matching. These expressions also describe the behavior of the system, concerning power absorption at the neighborhood of the impedance matching.

Our findings not only reaffirm the potential of integrating advanced mathematical techniques in automotive engineering but also open new perspectives for future research.

Author Contributions: Conceptualization: A.H., S.A. and J.L.O.; data curation: A.H., S.A. and J.D.A.; formal analysis: A.H., J.L.O. and S.A.; investigation: A.H., J.L.O., S.A. and J.D.A.; methodology: A.H., S.A. and J.D.A.; resources: J.L.O., A.H. and S.A.; supervision: A.H., J.L.O. and S.A.; validation: S.A., A.H., J.D.A. and M.Á.G.; software: J.D.A.; visualization: J.D.A. and M.Á.G.; writing—original draft: J.L.O., A.H., S.A. and J.D.A.; writing—review and editing: A.H., S.A., J.D.A., J.L.O. and M.Á.G. All authors have read and agreed to the published version of the manuscript.

Funding: This research received no external funding.

Data Availability Statement: Not applicable.

Conflicts of Interest: The authors declare no conflicts of interest.

Appendix A

Figure 2 shows the case of a rectangular magnet with a square cross section glued to the free end of a cantilever that oscillates around its equilibrium position. In that position, the poles of the magnet are in front of a square coil surface with the same dimensions, in such a way that the flux through the coil surface is at its maximum, i.e., $\Phi(0)$ in (8) is the maximum. After again assuming that the magnetic field lines, B, are restricted to the magnet surface, the flux through the n-turns coil becomes $nBS(x)$, where $S(x)$ is given by $S(x) = a(a - |x|)$, a being the square side.

In this case, Equation (18) changes to

$$x'' + \left(\gamma + \frac{n^2B^2}{m(R+R^*)}a^2\right)x' + \omega_0^2 x = \int_{-\infty}^{\infty} F(\omega)cos\omega t\, d\omega \quad \text{(A1)}$$

This equation is analytical, and its solution is the standard one corresponding to a harmonic oscillator.

Appendix B

In this article, in Figure 3 for example, the solutions to two differential equations are compared: the original Equation (19) and the linear approximation (20). These solutions are obtained using the Runge–Kutta ode89 method, included in Matlab:

- Original equation, nonlinear

$$x'' + \left[\gamma + \frac{n^2B^2}{m(R+R^*)}(4r^2 - x^2)\right]x' + \omega_0^2 x = F_0 \cos\omega t \quad (x \le 2r) \text{ (A2)}$$

$$x'' + \gamma x' + \omega_0^2 x = F_0 \cos\omega t \quad (x > 2r) \text{ (A3)}$$

- Approximated equation, linear

$$x'' + \left[\gamma + \frac{n^2B^2}{m(R+R^*)}(4r^2)\right]x' + \omega_0^2 x = F_0 \cos \omega t \quad (x \le 2r) \quad \text{(A4)}$$

$$x'' + \gamma x' + \omega_0^2 x = F_0 \cos \omega t \quad (x > 2r) \quad \text{(A5)}$$

Using the parameters:

r = 0.005 m
n = 1000
B = 1 T
M = 2 kg
$R + R^*$ = 20 Ω
γ = 4 N·s/kg·m
$\omega_0 = 2\pi \times 20$ [rad/s]
$F(\omega) = \omega_0^2 x_{l,\omega} = (2\pi \times 20)^2 \times 0.005$

In all cases $x(0) = x'(0) = 0$ as initial conditions
The value for the fit parameter α mentioned in the article is 4.

- Overlapping approximate and original solutions for ω = 0.1 Hz (Figures A1 and A2):

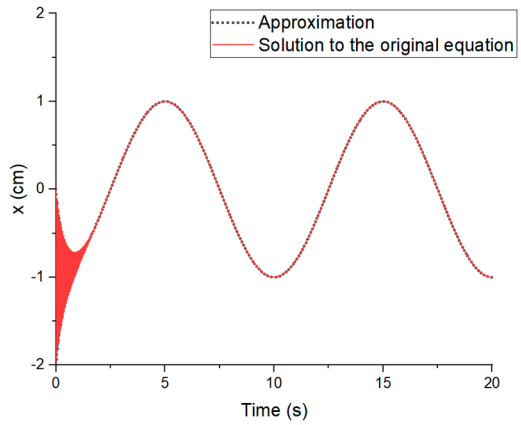

Figure A1. Comparison between approximation and original solution to the equation for ω = 0.1 Hz between 0 and 20 s.

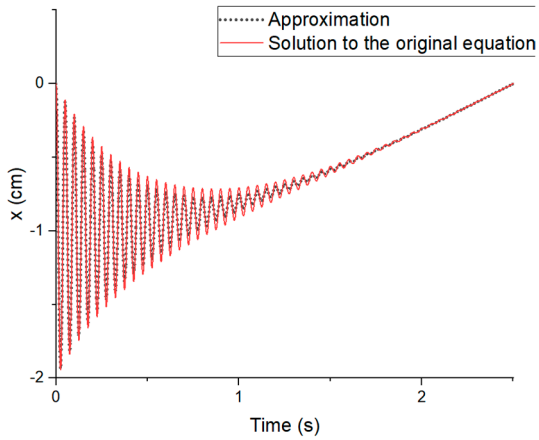

Figure A2. Comparison between approximation and original solution to the equation for ω = 0.1 Hz between 0 and 2 s (more zoom than in the previous figure).

As we are far and below ω_0, the amplitude is close to 1 cm ($2r$). Closer to the ω_0 (20 Hz), the amplitude grows a lot for the same applied force, and then decreases towards 0 with ω. If we plot sweeps of ω:

- Maximum difference between both solutions in stationary state:
  - From 5 Hz up to 100 Hz (Figure A3):

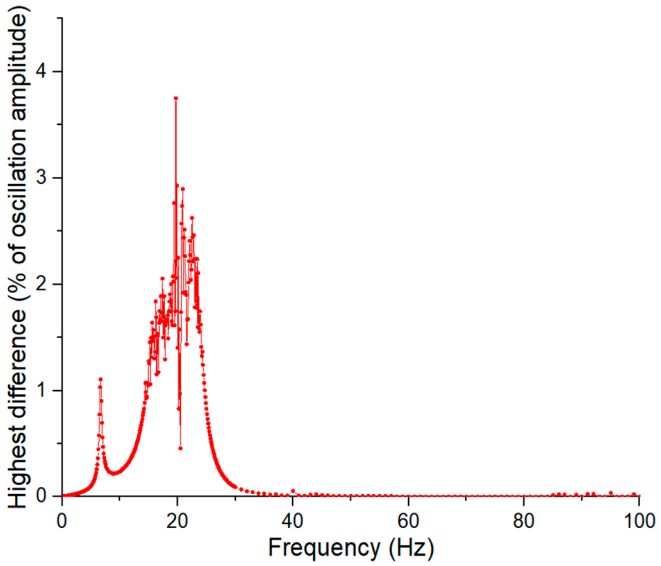

Figure A3. Difference in amplitude between approximation equation and original equation of solution in stationary state, from 5 Hz up to 100 Hz.

  - From 10 to 30 Hz (Figure A4):

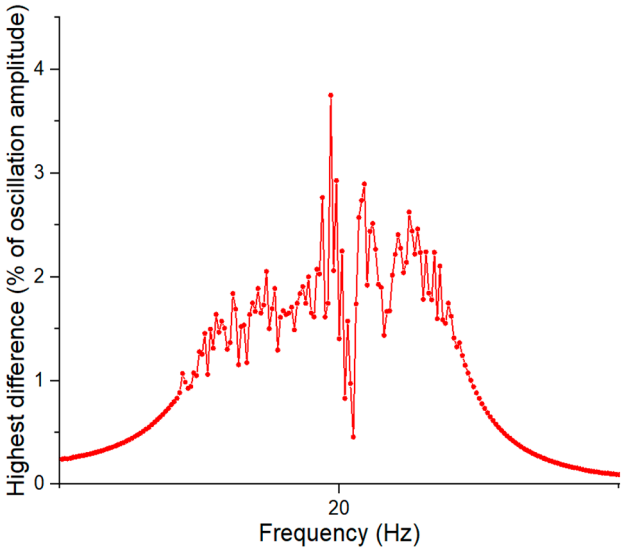

Figure A4. Difference in amplitude between approximation equation and original equation of solution in stationary state, from 10Hz up to 30Hz.

As can be seen in the previous graphs, the maximum difference in amplitude between the original solution and the approximate solution does not reach 4%, so it can be concluded that it is a good simplification, being valid and representative of the original solution.

References

1. Energía y Sociedad-EVE. Available online: https://www.eve.eus/Conoce-la-Energia/Que-sabes-de/Energia-y-sociedad?lang=en-en (accessed on 27 June 2022).
2. AIHE (Asociación de la Industria Hidrocarbullera del Ecuador) EL PETRÓLEO EN CIFRAS 2020. Available online: https://www.aihe.org.ec/wp-content/uploads/2021/04/PETROLEO-EN-CIFRAS-2020-WEB-OK.pdf (accessed on 1 September 2022).
3. Zhang, R.; Wang, X.; John, S. A Comprehensive Review of the Techniques on Regenerative Shock Absorber Systems. *Energies* **2018**, *11*, 1167.
4. Li, L.; Zhang, Y.; Yang, C.; Yan, B.; Marina Martinez, C. Model Predictive Control-Based Efficient Energy Recovery Control Strategy for Regenerative Braking System of Hybrid Electric Bus. *Energy Convers. Manag.* **2016**, *111*, 299–314.
5. Liu, X.; Li, C.; Deng, Y.D.; Su, C.Q. An Energy-Harvesting System Using Thermoelectric Power Generation for Automotive Application. *Int. J. Electr. Power Energy Syst.* **2015**, *67*, 510–516.
6. Saidur, R.; Rezaei, M.; Muzammil, W.K.; Hassan, M.H.; Paria, S.; Hasanuzzaman, M. Technologies to Recover Exhaust Heat from Internal Combustion Engines. *Renew. Sustain. Energy Rev.* **2012**, *16*, 5649–5659.
7. Lee, J.; Choi, B. Development of a Piezoelectric Energy Harvesting System for Implementing Wireless Sensors on the Tires. *Energy Convers. Manag.* **2014**, *78*, 32–38.
8. Múčka, P. Energy-Harvesting Potential of Automobile Suspension. *Veh. Syst. Dyn.* **2016**, *54*, 1651–1670.
9. Imaduddin, F.; Mazlan, S.A.; Zamzuri, H. A Design and Modelling Review of Rotary Magnetorheological Damper. *Mater. Des.* **2013**, *51*, 575–591.
10. Ahamed, R.; Ferdaus, M.M.; Li, Y. Advancement in Energy Harvesting Magneto-Rheological Fluid Damper: A Review. *Korea Aust. Rheol. J.* **2016**, *28*, 355–379.
11. Hu, G.; Lu, Y.; Sun, S.; Li, W. Performance Analysis of a Magnetorheological Damper with Energy Harvesting Ability. *Shock Vib.* **2016**, *2016*, 2959763.
12. Huang, C.; Yao, J.; Zhang, T.; Chen, Y.; Jiang, H.; Li, D. Damping Applications of Ferrofluids: A Review. *J. Magn.* **2017**, *22*, 109–121.
13. Li, Y.; Han, P.; Li, D.; Chen, S.; Wang, Y. Typical Dampers and Energy Harvesters Based on Characteristics of Ferrofluids. *Friction* **2022**, *11*, 165–186.
14. Lenkutis, T.; Viržonis, D.; Cerškus, A.; Dzedzickis, A.; Šešok, N.; Bučinskas, V. An Automotive Ferrofluidic Electromagnetic System for Energy Harvesting and Adaptive Damping. *Sensors* **2022**, *22*, 1195.
15. Xie, X.D.; Wang, Q. Energy Harvesting from a Vehicle Suspension System. *Energy* **2015**, *86*, 385–392.
16. Sapiński, B. Energy-Harvesting Linear MR Damper: Prototyping and Testing. *Smart Mater. Struct.* **2014**, *23*, 035021.
17. Li, Z.; Zuo, L.; Luhrs, G.; Lin, L.; Qin, Y. Electromagnetic Energy-Harvesting Shock Absorbers: Design, Modeling and Road Tests. *IEEE Trans. Veh. Technol.* **2013**, *62*, 1065–1074.
18. Amati, N.; Festini, A.; Tonoli, A. Design of Electromagnetic Shock Absorbers for Automotive Suspensions. *Veh. Syst. Dyn.* **2011**, *49*, 1913–1928.
19. Xu, L.; Fang, Z.; Guo, X.; Zhang, H. An Optimal Algorithm for Energy Recovery of Hydraulic Electromagnetic Energy-Regenerative Shock Absorber. *Appl. Math. Inf. Sci.* **2013**, *7*, 2207–2214.
20. Galluzzi, R.; Tonoli, A.; Amati, N. Modeling Control and Validation of Electrohydrostatic Shock Absorbers. *J. Vib. Acoust.* **2015**, *137*, 011012.
21. Bowen, L.; Vinolas, J.; Olazagoitia, J.L. Methodology for Comparing the Functional Performance of Energy Harvesting Shock Absorbers. *Int. J. Appl. Electromagn. Mech.* **2017**, *55*, 545–564.
22. Aberturas, S.; Hernando, A.; Olazagoitia, J.L.; García, M.Á. Study of an Energy-Harvesting Damper Based on Magnetic Interaction. *Sensors* **2022**, *22*, 7865. https://doi.org/10.3390/s22207865.
23. Xiong, L.; Gao, S.; Jin, L.; Guo, S.; Sun, Y.; Liu, F. The Design and Experiment of a Spring-Coupling Electromagnetic Galloping Energy Harvester. *Micromachines* **2023**, *14*, 968. https://doi.org/10.3390/mi14050968.
24. Jiang, W.; Song, Y.; Xu, Y.; Zhou, R.; Sun, F.; Zhang, X. Energy-Harvesting Characteristics of a Dual-Mode Magnetic Suspension for Vehicles: Analysis and Experimental Verification. *Actuators* **2022**, *11*, 363. https://doi.org/10.3390/act11120363.
25. Aberturas, S.; Olazagoitia, J.L.; García, M.Á.; Hernando, A. Enhanced Energy Recovery in Magnetic Energy-Harvesting Shock Absorbers Using Soft Magnetic Materials. *Magnetochemistry* **2023**, *9*, 189. https://doi.org/10.3390/magnetochemistry9070189.
26. Chikazumi, S. *Physics of Ferromagnetism*; Oxford Press: New York, NY, USA, 1997.